Supporting Information for Universality in Nonaqueous Alkali Oxygen Reduction on Metal Surfaces: Implications for Li-O_2 and Na-O_2 Batteries

Dilip Krishnamurthy,[†] Heine Anton Hansen,[‡] and Venkatasubramanian Viswanathan[*,†]

†*Department of Mechanical Engineering, Carnegie Mellon University, Pittsburgh, Pennsylvania, 15213*

‡*Department of Energy Conversion and Storage, Technical University of Denmark, Kgs. Lyngby DK-2800, Denmark*

E-mail: venkvis@cmu.edu

The document includes computational details, quantifying uncertainty in adsorption energies, scaling relationships and activity volcano plots for Li-O_2 and Na-O_2 electrochemistry.

Computational Details

Density functional theory (DFT) calculations are carried out using GPAW[1] with BEEF-vdW[2] as the exchange-correlation functional using the Atomic Simulation Environment (ASE).[3] All calculations were done with a grid spacing of 0.18 Å, and converged with a force criterion of < 0.05 eV/Å. A $4 \times 4 \times 1$ k-point grid was used for a unit cell having 3 atoms each in the x and y directions and with 4 layers in the z-direction ($3 \times 3 \times 4$). The bottom two layers of the slab were fixed and the remaining were allowed to be relaxed. For other types of unit cells considered in the calculation, the k-points were suitably scaled. All structures were converged with a force criterion of < 0.05 eV/Å.

Quantifying Uncertainty in Adsorption Energies

The recently developed exchange correlation functional, BEEF-vdW (Bayesian Error Estimation Functional),[2] allows us to use its unique error estimation capability[2] to quantify error in adsorption energies. The method uses different types of data sets as the empirical data and fits the GGA exchange enhancement factor, $F_x(s)$ to it.

The expression for the Exchange correlation energy for BEEF-vdW is given by,

$$E_{xc} = \sum_{m=0}^{M_x-1} a_m E_m^{GGA-x} + \alpha_c E^{LDA-c} + (1-\alpha_c) E^{PBE-c} + E^{nl-c}. \quad (1)$$

Where, M_x represents the degree of the polynomial. The coefficients a_m and α_c are the fitting parameters which are optimized over the data sets. E_m^{GGA-x} represents the GGA exchange energy, E^{PBE-c} and E^{LDA-c} represent the PBE and LDA correlation energies and E^{nl-c} represents the non-local correlation energy obtained from the functional vdW-DF2 .[4]

BEEF-vdW uses an ensemble of functionals to calculate errors.[5] After calculating the optimum value for the coefficients a_m and α_c, each coefficient is perturbed around its optimal value. From the ensemble of coefficients an ensemble of energies (eq 1) is generated. The ensemble of energies provides a systematic way to calculate the uncertainty associated within the GGA class of functionals for a given calculation. This approach provides a computationally tractable way to estimate the uncertainty associated with a given calculation.

Following this approach, an ensemble of exchange correlation functionals results in an ensemble of adsorption energies, from which the error in the adsorption energy is obtained as the sensitivity of DFT results to the choice of the exchange-correlation functional. Figures S1 and S2 show the ensemble of adsorption energies obtained for LiO_2^* and NaO_2^* respectively, with the corresponding normalized frequency.

Using the BEEF-vdW functional, ensembles of adsorption energies for various intermediates involved in the ORR were calculated. Referencing the adsorption energy of any intermediate with respect to gas phase molecules (here O_2(g)) leads to large estimated error. However, when the reference is changed from the gas phase molecules to a reference element, for e.g., Pt(111), it is found that this leads to much smaller error estimates due to similarity in metal-adsorbate bonding characteristics. This is in agreement with the notion that trends in DFT calculations are more accurate than the individual values due to cancellation of systematic errors. We use the following methodology to get a combined error estimate for the adsorption energies of various intermediates. We illustrate the approach using the example of the intermediate LiO_2^*.

First the ensemble of LiO_2^* adsorption energy for a given metal facet 'X' with respect to a reference system, chosen as Pt(111), is calculated. This is given by

$$\Delta G_{LiO_2}(X|Pt(111)) = \Delta G_{LiO_2}(X) - \Delta G_{LiO_2}(Pt(111)) \tag{2}$$

The distribution for the calculated ensemble of adsorption energies is centered around the

mean:

$$\overline{\Delta G_{LiO_2}(X|Pt(111))} = \Delta G_{LiO_2}(X|Pt(111)) - \langle \Delta G_{LiO_2}(X|Pt(111)) \rangle. \quad (3)$$

We carry out for all the fcc metal (111) and (100) facets considered in this study and a combined distribution is constructed:

$$\Delta G_{LiO_2} = \sum_X \overline{\Delta G_{LiO_2}(X|Pt(111))} \quad (4)$$

Figure S1 shows the combined adsorption energy distribution for the intermediate LiO_2^* ($\Delta G_{LiO_2^*}$) calculated for metal facets Ag(111), Au(111), Au(100), Ag(100), -0.5%-Pt(111), -1%-Pt(111), -1.5%-Pt(111) and -2%-Pt(111), relative to Pt(111). In all, the distribution contains 20000 values, 2000 for each metal facet considered. The standard deviation for the distribution (σ_{LiO_2}) is 0.27 eV.

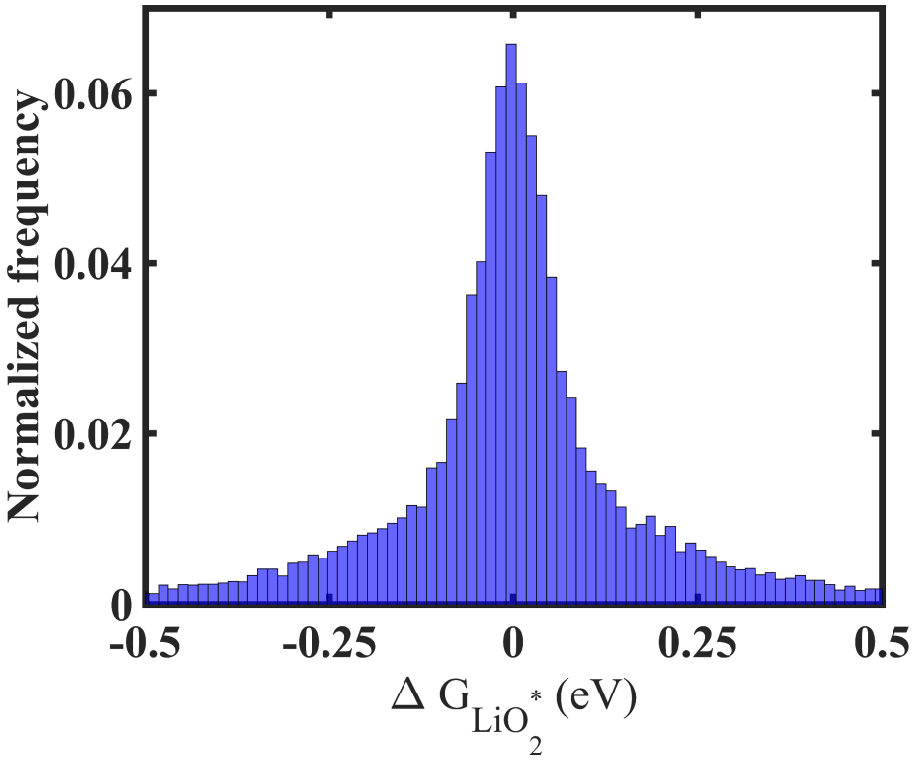

Figure S1: Normalized frequency as a function of the adsorption energy (mean shifted to 0) of the intermediate, LiO_2^*, obtained from Ag(111), Au(111), Ag(100), Au(100), -0.5%-Pt(111), -1%-Pt(111), -1.5%-Pt(111) and -2%-Pt(111), relative to Pt(111). The standard deviation of the combined ensemble, $\sigma_{LiO_2^*}$ = is 0.27 eV.

Similarly, Figure S2 shows the combined adsorption energy distribution for the intermediate NaO_2^* ($\Delta G_{NaO_2^*}$) calculated for metal facets Ag(111), Au(111), Au(100) and Ag(100) relative to Pt(111). The standard deviation for the distribution (σ_{NaO_2}) is 0.31 eV. The distribution for the case of LiO_2^* is tighter due to the ensemble of adsorption energies on the strained Pt(111) facets.

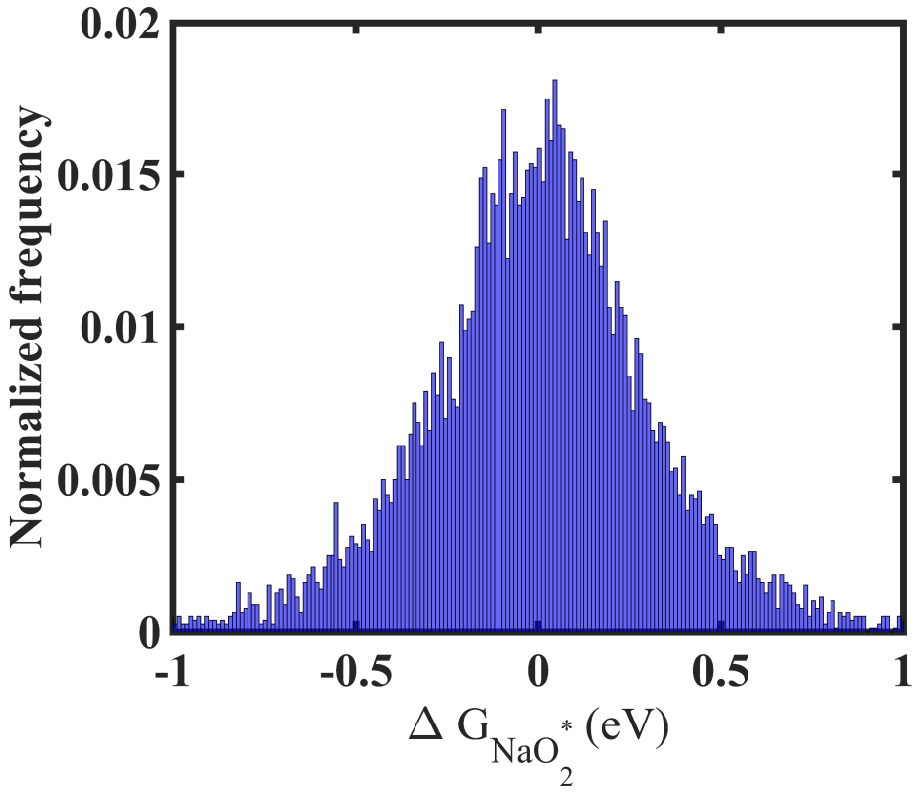

Figure S2: Normalized frequency as a function of the adsorption energy (mean shifted to 0) of the intermediate, NaO_2^*, obtained from Ag(111), Au(111), Ag(100) and Au(100), relative to Pt(111). The standard deviation of the combined ensemble, $\sigma_{NaO_2^*}$ = is 0.31 eV.

Based on this analysis, we approximate the uncertainty involved in determining the adsorption energy of an intermediate by the the standard deviation of the calculated adsorption energy ensemble on the various metal facets. In the next section, we discuss how the obtained uncertainty translates to uncertainty in the limiting potential in the volcano plots.

Scaling relationships

It has been shown that there exists a linear scaling between the adsorption energies of the hydrogenated species, AH_x and the atom A.[6] Using simple bond counting principles it was shown that the slope of the linear scaling is only dependent on the valency and not on the specific metal facet considered.[7]

We explore the trends in adsorption energy between LiO_2^* and LiO^*, and observe that the adsorption free energies between LiO_2^* and LiO^* scale with each other independent of the metal facet considered. Similarly, we observe a linear scaling between NaO_2^* and NaO^* irrespective of the metal facet considered. We explore the uncertainty in the intercept of the scaling relationship between the adsorption energies of the adsorbates LiO^* and LiO_2^* as well as between adsorbates NaO^* and NaO_2^*. As mentioned in the main text, we assume that the slope between the adsorption energies of the intermediates is one. This arises due to arguments based on the bond order conservation principle.[6]. Fig. S3 and Fig. S4 show the best-fit lines, which have R-squared values extremely close to the slope-1 lines.

The expression for the standard deviation of the scaling intercept used is derived in the

following way:

$$(\sigma_{\mathrm{X-Y}})^2 = \mathrm{E}[(\mathrm{X}-\mathrm{Y})^2] - (\mathrm{E}[(\mathrm{X}-\mathrm{Y})])^2 \tag{5a}$$

$$(\sigma_{\mathrm{X-Y}})^2 = \mathrm{E}[\mathrm{X}^2 + \mathrm{Y}^2 - 2\mathrm{XY}] - (\mathrm{E}[\mathrm{X}] - \mathrm{E}[\mathrm{Y}])^2 \tag{5b}$$

$$(\sigma_{\mathrm{X-Y}})^2 = \mathrm{E}[\mathrm{X}^2] + \mathrm{E}[\mathrm{Y}^2] - 2\mathrm{E}[\mathrm{XY}] - (\mathrm{E}[\mathrm{X}])^2 - (\mathrm{E}[\mathrm{Y}])^2 + 2\mathrm{E}[\mathrm{X}]\mathrm{E}[\mathrm{Y}] \tag{5c}$$

$$(\sigma_{\mathrm{X-Y}})^2 = (\sigma_{\mathrm{X}})^2 + (\sigma_{\mathrm{Y}})^2 - 2(\mathrm{E}[\mathrm{XY}] - \mathrm{E}[\mathrm{X}]\mathrm{E}[\mathrm{Y}]) \tag{5d}$$

$$(\sigma_{\mathrm{X-Y}})^2 = (\sigma_{\mathrm{X}})^2 + (\sigma_{\mathrm{Y}})^2 + (\mu_{\mathrm{XY}} - \mu_{\mathrm{X}}\mu_{\mathrm{Y}}) \tag{5e}$$

This relation derived above from statistics, holds for any two random variables X and Y. The relation, $\sigma^2_{(\mathrm{LiO^*-LiO^*_2})} = \sigma^2_{\mathrm{LiO^*}} + \sigma^2_{\mathrm{LiO^*_2}} - 2(\mu_{(\mathrm{LiO^*LiO^*_2})}$ - $\mu_{\mathrm{LiO^*}}\mu_{\mathrm{LiO^*_2}})$, was used to generate the standard deviation of the intercept, where $\sigma_{\mathrm{LiO^*}}$, $\mu_{\mathrm{LiO^*}}$ and $\sigma_{\mathrm{LiO^*_2}}$, $\mu_{\mathrm{LiO^*_2}}$ are the standard deviations and mean values for $\Delta\mathrm{G}_{\mathrm{LiO^*}}$ and $\Delta\mathrm{G}_{\mathrm{LiO^*_2}}$. $\mu_{\mathrm{LiO^*LiO^*_2}}$ is the mean associated with the distribution of $\Delta G_{\mathrm{LiO^*}} \times \Delta G_{\mathrm{LiO^*_2}}$. $\sigma_{(\mathrm{LiO^*-LiO^*_2})}$ is the standard deviation for the scaling relationship.

Scaling between the free energies of $\mathrm{LiO^*_2}$ and $\mathrm{LiO^*}$, with the best-fit regression line

Fig. S3 shows the best-fit regression line, which has an R^2 value of 0.93. The regression line (shown in black bold) is obtained by fitting the adsorption energies on Pt(111), -0.5%−Pt(111),-1%−Pt(111),-1.5%−Pt(111),-2%−Pt(111), Au(111), Ag(111), Au(100) and Ag(100). On considering a slope of 1 based on bond conservation principles, we observe an R^2 value that's extremely close to the best-fit line as reported in the main text.

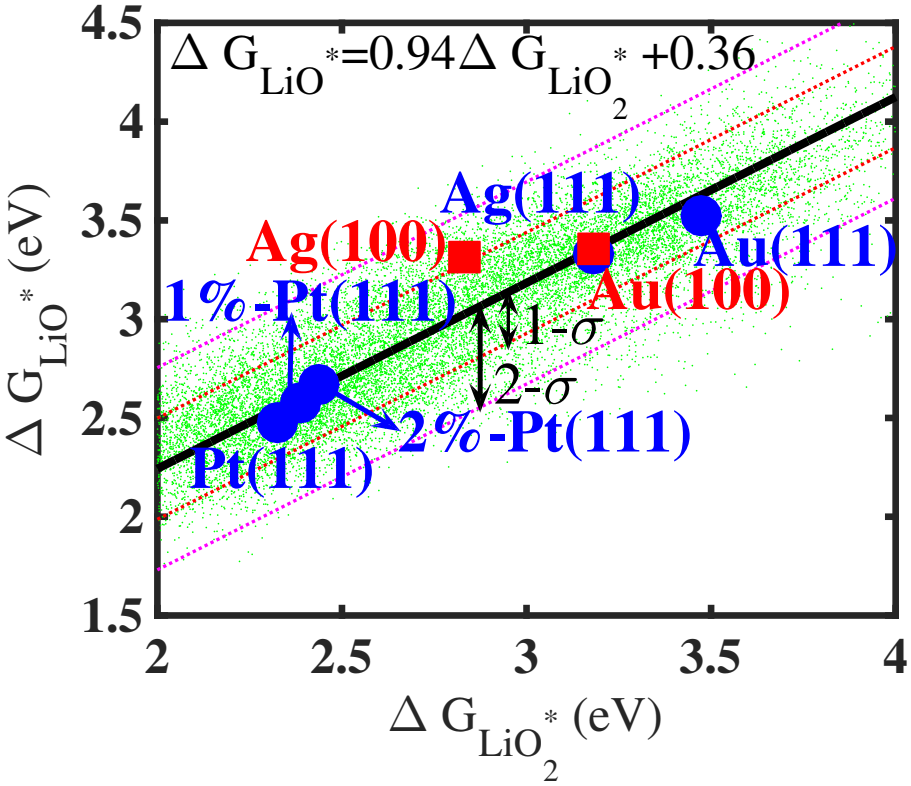

Figure S3: Best-fit linear line with adsorption energies of LiO_2^* and LiO^* on Pt(111), -0.5%−Pt(111),-1%−Pt(111),-1.5%−Pt(111),-2%−Pt(111), Au(111), Ag(111), Au(100) and Ag(100). The slope (0.94) is close to slope 1 as expected from bond conservation principles. The R^2 value for the best-fit line is 0.93 (same as the slope-1 line).

Scaling between the free energies of NaO_2^* and NaO^*, with the best-fit regression line

Fig. S4 shows the best-fit regression line, which has an R^2 value of 0.98. The regression line (shown in black bold) is obtained by fitting the adsorption energies on Pt(111), Au(111), Ag(111), Au(100) and Ag(100). On considering a slope of 1 based on bond conservation principles, we observe an R^2 value that's extremely close to the best-fit line as reported in the main text.

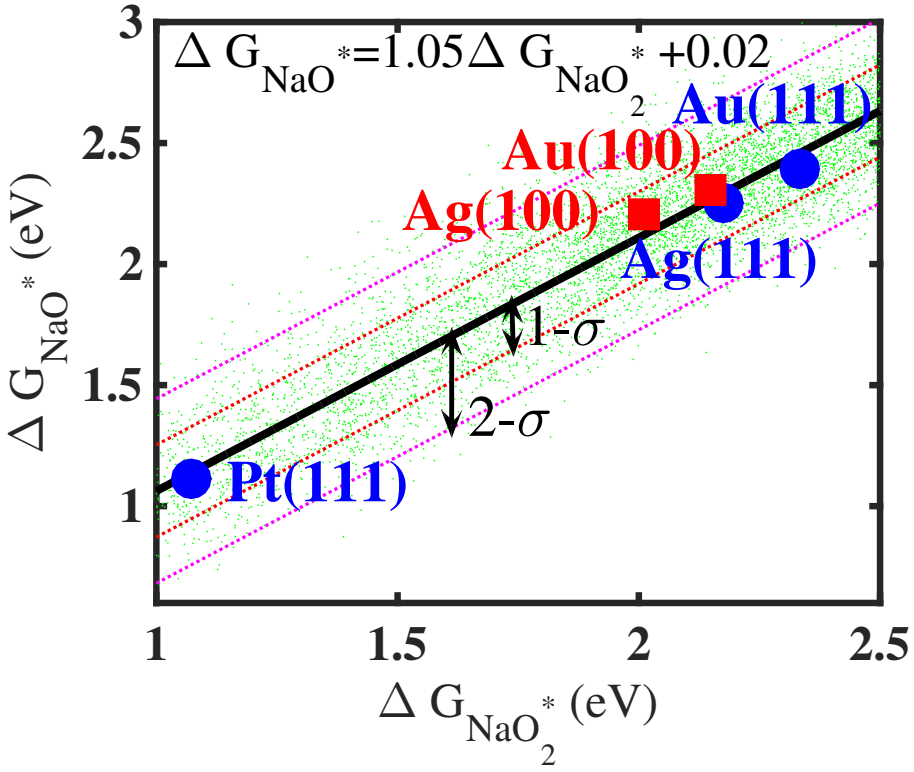

Figure S4: Best-fit linear line with adsorption energies of NaO_2^* and NaO^* on Pt(111), Au(111), Ag(111), Au(100) and Ag(100). The slope (1.05) is close to slope 1 as expected from bond conservation principles. The R^2 value for the best-fit line is 0.98 (same as the slope-1 line).

Volcano Plots for Li-O_2 electrochemistry

In this section, volcano plots are discussed for the $2e^-$ oxygen reduction to Li_2O_2 in the case of the Li-O_2 battery and the $1e^-$ reduction to Na_2O in the case of the Na-O_2 battery, based on the primary discharge product. In Fig. S5, the limiting potential (bold black line) is plotted as a function of the descriptor, $G_{LiO_2^*}$ relative to Pt(111). The red dots represent the 100 facets and the blue dots represent the 111 facets. The black dotted lines represent the 1-σ bounds (uncertainty) obtained from the combined ensemble of adsorption energies of $\Delta G_{LiO_2^*}$.

Activity volcano for the $2e^-$ reduction to Li_2O_2 with 1σ bounds

Fig. S5 shows the limiting potential (black bold) with uncertainty (1σ) bounds (black dotted lines). The highest limiting potential possible for the Li-O_2 battery is 2.96 V vs. the Li/Li^+ reference electrode, which fixes the bound for the black dotted lines near the top of the volcano.

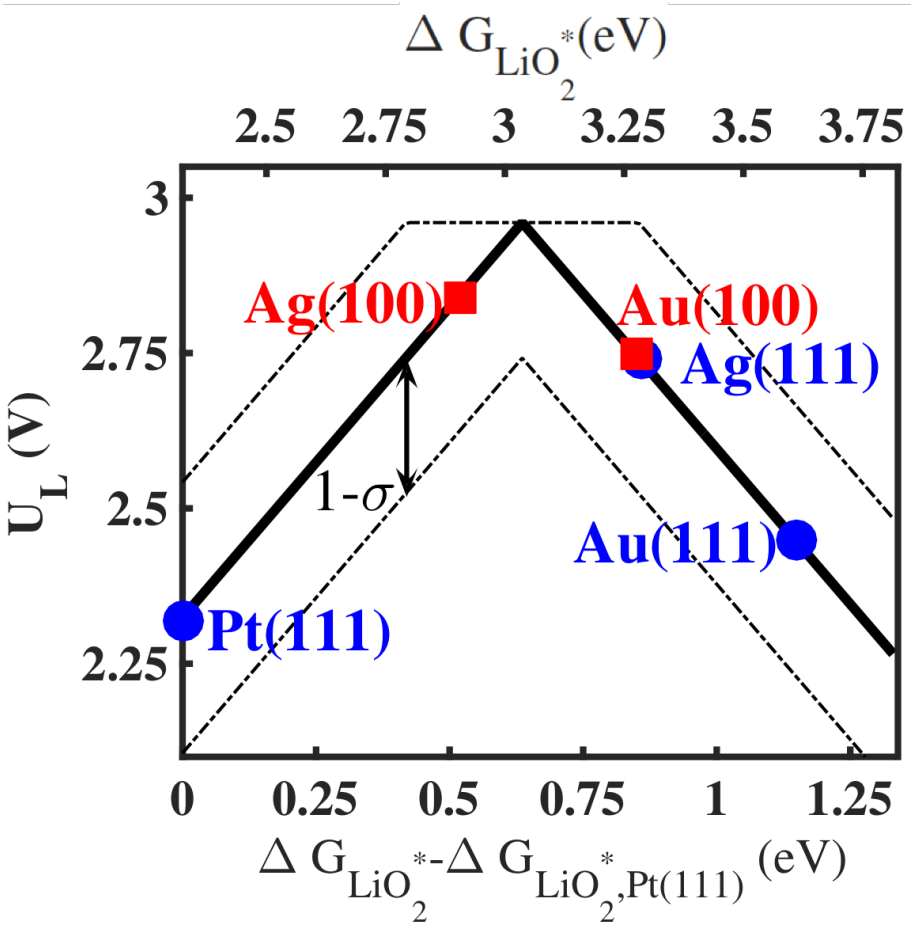

Figure S5: Limiting potential as a function of the free energy of LiO_2^* with respect to that on Pt(111). The black dotted lines represents the 1σ limit for the limiting potential for any given adsorption energy value.. The standard deviation (σ) is calculated from an ensemble of adsorption energies on Pt(111), -0.5%−Pt(111),-1%−Pt(111),-1.5%−Pt(111),-2%−Pt(111), Au(111), Ag(111), Au(100) and Ag(100).

Activity volcano for the $2e^-$ reduction to Li_2O_2 with error bars

As discussed in the section on quantifying uncertainty , for each metal facet, the uncertainty is calculated from the ensemble of adsorption energies with respect to Pt(111). For a metal facet, 'X', the standard deviation of the distribution, $\Delta G_{LiO_2}(X|Pt(111))$ (refer eqn. 2) is approximated as the uncertainty, which is represented by the error bars in Fig. S6.

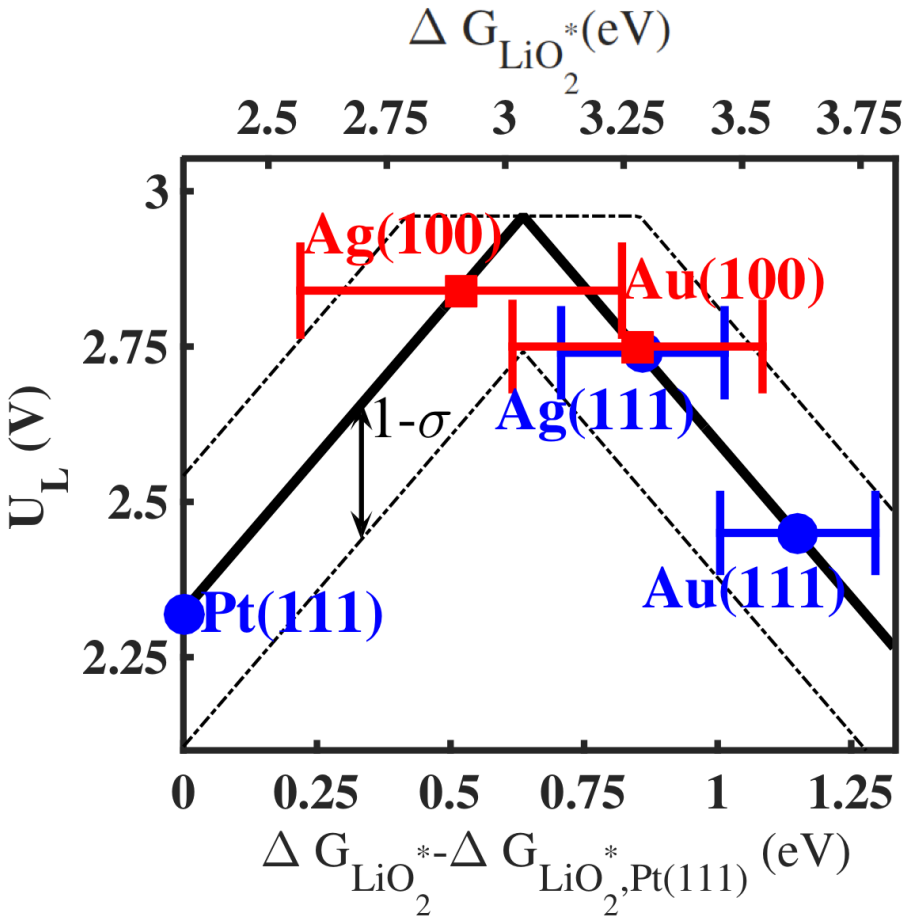

Figure S6: Limiting potential as a function of the free energy of LiO_2^* with respect to that on Pt(111). The error bars show standard deviation in the adsorption energies on each metal facet. For each metal facet, the uncertainty is calculated as the standard deviation of the ensemble of adsorption energies on the respective metal surface relative to that on Pt(111) (Refer eqn. 2)

.

Activity volcano for the $2e^-$ reduction to Li_2O_2, showing the expected limiting potential (U_{EL})

The uncertainty is predicted using a parameter that we define as the expected limiting potential, U_{EL}, which is the expected value of U_L. The deviation of the expected limiting potential, U_{EL}, from the thermodynamic limiting potential, U_L is a qualitative estimate of the prediction uncertainty and can be used to identify trends in predictability. We notice that the expected limiting potential, U_{EL}, and the limiting potential, U_L deviate from each other close to the top of the activity volcano, which implies that the activity predictions from the thermodynamic activity volcano become less reliable in this region. Figures S5 and S6 provide a way to understand the uncertainties associated with the limiting potentials, however, they do not provide a visual representation of the probability distribution associated with the limiting potential, U_L.

To determine the probability distribution, we first determine the probability distribution for the limiting potential U_L as a function of the free energy of the intermediate LiO_2^* relative to Pt(111). Then, we consider a random variable $\Delta G_{LiO_2^*} \sim N(\langle \Delta G_{LiO_2^*} \rangle, \sigma_{LiO_2^*})$ where, $\langle \Delta G_{LiO_2^*} \rangle$ is the mean and $\sigma_{LiO_2^*}$ is the standard deviation corresponding to the adsorption energy of the intermediate, LiO_2^*. A given value of the mean, $\langle \Delta G_{LiO_2^*} \rangle$ represents a calculated value of the free energy while the random variable, $\Delta G_{LiO_2^*}$, accounts for the uncertainty of the calculated value. This gives rise to a probability distribution of the limiting potential, U_L as a function of the mean, $\langle \Delta G_{LiO_2^*} \rangle$. From the probability distribution, the expected limiting potential (U_{EL}) is derived, which is the expectation value of the limiting potential, U_L. For a given value of $\langle \Delta G_{LiO_2^*} \rangle$, the expected limiting potential represents the value that would be expected given a large number of experiments on materials with the same calculated value.

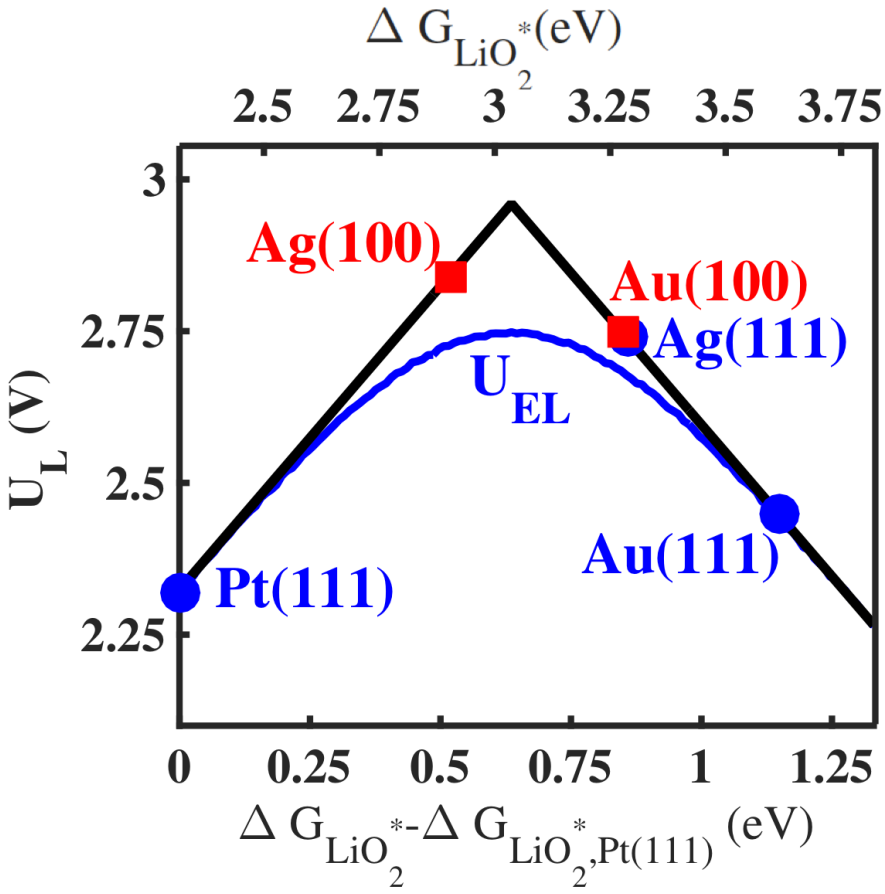

Figure S7: Limiting potential as a function of the free energy of LiO_2^* with respect to that on Pt(111). The blue line shows the expected limiting potential. Points near the top of the volcano are associated with a higher uncertainty compared to the other points

Sabatier volcano for the 1e$^-$ reduction of O_2 to Na_2O involving a chemical nucleation step

Since there is a chemical step involved, we perform a Sabatier analysis[8] to determine the activity of materials. For chemical steps, the upper limit to the forward rate is given by[9]

$$r_C = \frac{k_B T}{h} \exp\Big(- \frac{\Delta G}{k_B T} \Big) \tag{6}$$

where ΔG is the activation free energy. For electrochemical steps, due to the presence of solvent, there is an additional contribution from the requirement for the reorganization of solvent molecules around the reaction center undergoing the ion-coupled electron transfer. The rate of an electrochemical step is given by

$$r_{EC} = \frac{k_B T}{h} \exp\Big(- \frac{\lambda_{Na}}{k_B T} \Big) \exp\Big(- \frac{\Delta G_i}{k_B T} \Big) \tag{7}$$

The rate curves for the individual steps are shown in Fig. S8. It can be seen that the left leg is limited by the chemical step that involves the nucleation of NaO_2 from NaO_2^*. The plateau and the right leg are limited by the step involving the electrochemical activation of O_2 as NaO_2^*. Maximum current density is approached at the plateau when the electrochemical adsorption step becomes barrier-less. We observe that the nucleation rate (current density) for NaO_2 is highest on Au(111), Ag(111) and Au(100).

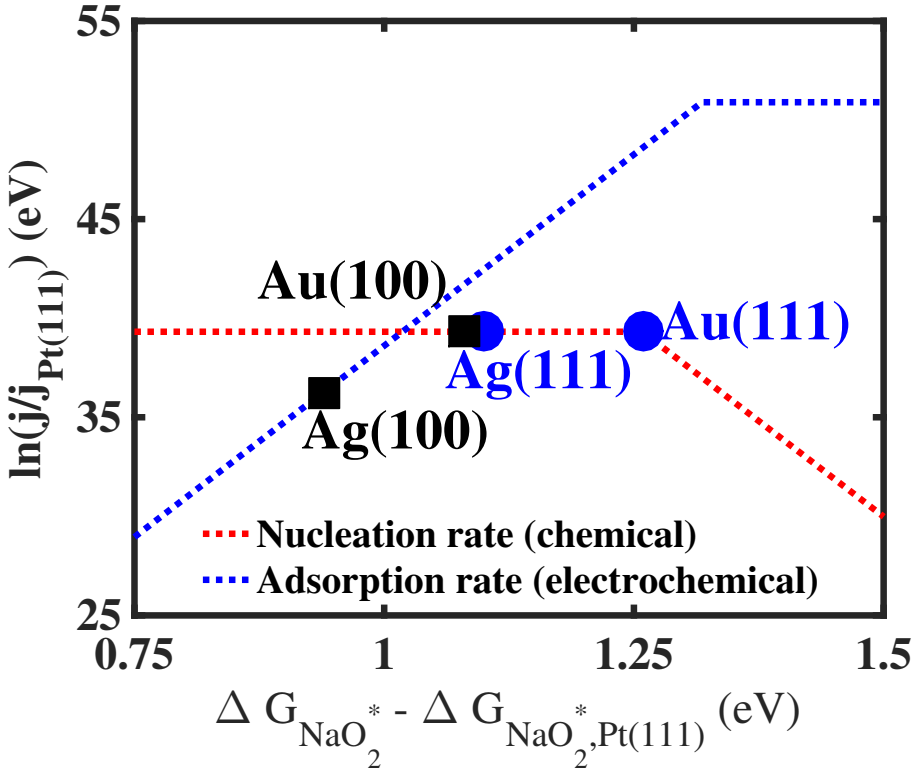

Figure S8: Sabatier volcano for the 1e$^-$ volcano. The current density relative to that on Pt(111) depends on the minimum rate of the two steps involved, the adsorption (electrochemical) step and the nucleation (chemical) step. The left leg is limited by the chemical step that involves the nucleation of NaO_2 from NaO_2^*. The plateau and the right leg are limited by the step involving the electrochemical activation of O_2 as NaO_2^*.

Volcano plots for Na-O_2 electrochemistry

Activity volcano for the 1e$^-$ reduction to NaO_2, for reorganization energies (λ_{Na}) of 0.1 eV, 0.3 eV and 0.5 eV

Fig. S9 shows the discharge current density for three different reorganization energies of solvents, 0.1 eV, 0.3 eV and 0.5 eV. As expected, an increase in the reorganization energy causes a lower current density due to a correspondingly higher energy barrier for the adsorption step. For the case of λ_{Na}=0.3 eV, we observe that the nucleation rate (current density) of NaO_2 on Au(111), Ag(111) and Au(100) is the highest and they lie in the plateau region.

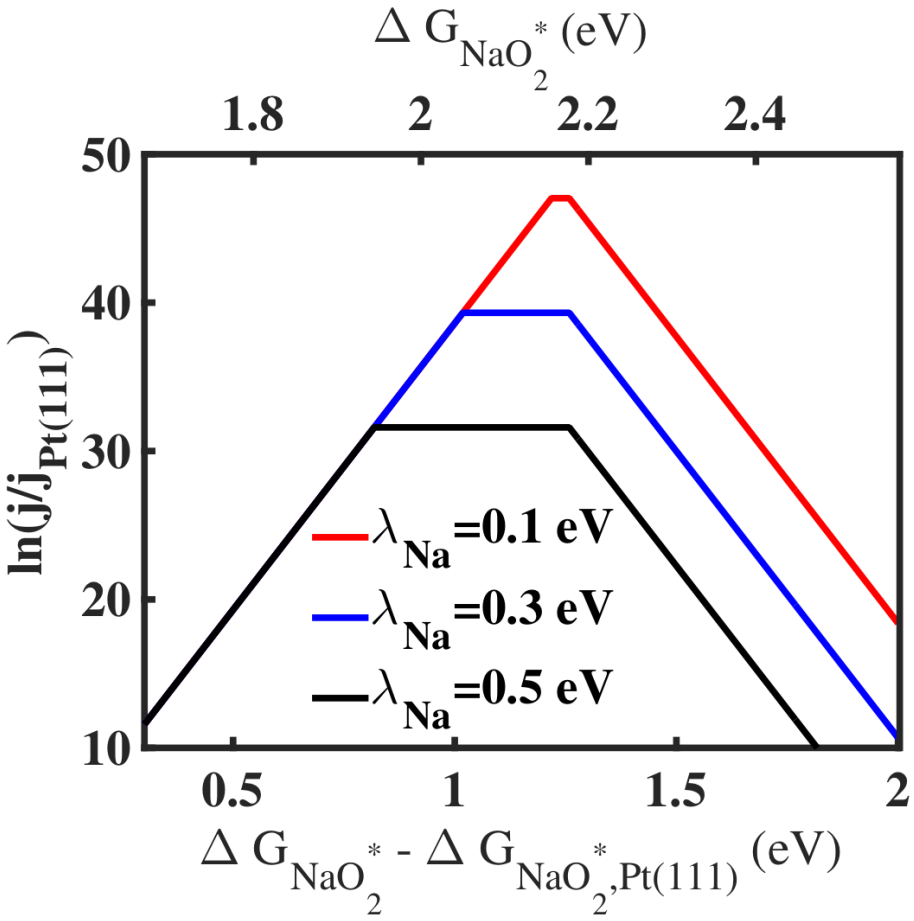

Figure S9: Current density normalized with respect to the current density on Pt(111) as a function of free energy of NaO_2^* with respect to that on Pt(111). Three cases of λ_{Na} are considered here to analyze the effect of different solvents. The left leg is limited by the chemical step that involves the nucleation of NaO_2 from NaO_2^*. The plateau and the right leg are limited by the step involving the electrochemical activation of O_2 as NaO_2^*. Maximum current density is approached at the plateau when the electrochemical adsorption step becomes barrier-less with highest adsorption rate. We observe that the nucleation rate (current density) of NaO_2 on Au(111), Ag(111) and Au(100) is the highest and they lie in the plateau region for λ_{Na}=0.3 eV

Activity volcano for the 1e$^-$ reduction to NaO_2 for λ_{Na} of 0.3 eV with error bars

As discussed in the section on quantifying uncertainty, for each metal facet, the uncertainty is calculated from the ensemble of adsorption energies with respect to Pt(111). For a metal facet, 'X', the standard deviation of the distribution, ΔG_{NaO_2}(X|Pt(111)) (refer eqn. 2) is approximated as the uncertainty, which is represented by the error bars in Fig. S10.

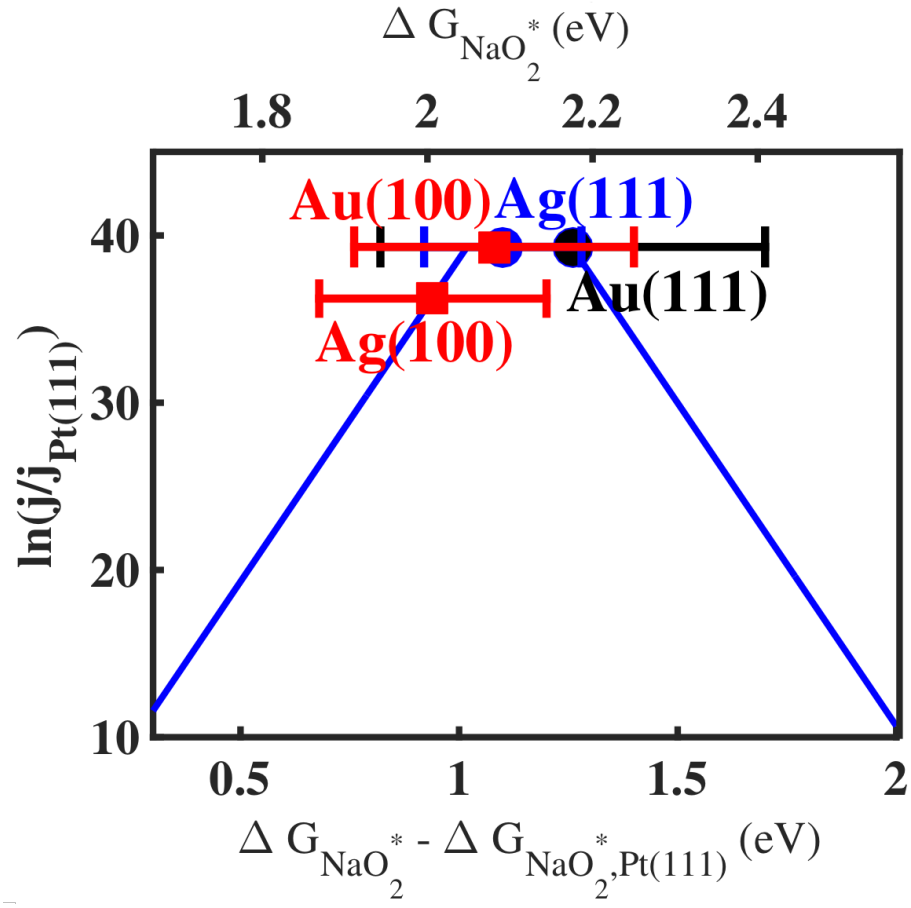

Figure S10: Current density normalized with respect to the current density on Pt(111) as a function of free energy of NaO_2^* with respect to that on Pt(111) for λ_{Na}=0.3 eV. The error bars show the standard deviation in the adsorption energies, calculated as the standard deviation of the ensemble of adsorption energies on the respective metal surface.

Activity volcano for the 1e$^-$ reduction to NaO_2 for λ_{Na} of 0.3 eV with 1σ bounds

Fig. S11 shows the limiting potential (blue bold) with uncertainty (1σ) bounds (black dotted lines).

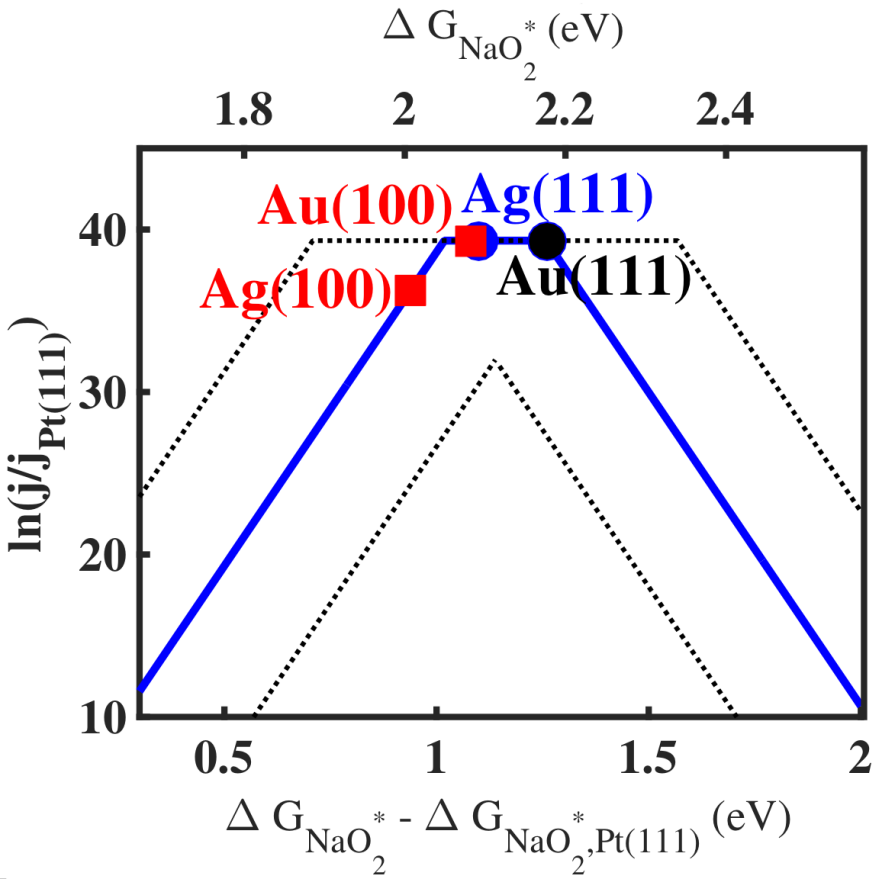

Figure S11: Current density normalized with respect to the current density on Pt(111) as a function of free energy of NaO_2^* with respect to that on Pt(111) for λ_{Na}=0.3 eV. The black dotted lines represents the 1σ limit. The standard deviation (σ) is calculated from an ensemble of adsorption energies on Pt(111), Au(111), Ag(111), Au(100) and Ag(100).

References

(1) Mortensen, J. J.; Hansen, L. B.; Jacobsen, K. W. Real-space grid implementation of the projector augmented wave method. *Phys. Rev. B* **2005**, *71*, 035109.

(2) Wellendorff, J.; Lundgaard, K. T.; Møgelhøj, A.; Petzold, V.; Landis, D. D.; Nørskov, J. K.; Bligaard, T.; Jacobsen, K. W. Density functionals for surface science: Exchange-correlation model development with Bayesian error estimation. *Phys. Rev. B* **2012**, *85*, 235149.

(3) Bahn, S. R.; Jacobsen, K. W. An object-oriented scripting interface to a legacy electronic structure code. *Comput. Sci. Eng.* **2002**, *4*, 56–66.

(4) Lee, K.; Murray, E. D.; Kong, L.; Lundqvist, B. I.; Langreth, D. C. Higher-Accuracy Van Der Waals Density Functional. *Phys. Rev. B* **2010**, *82*, 081101.

(5) Mortensen, J. J.; Kaasbjerg, K.; Frederiksen, S. L.; Norskov, J. K.; Sethna, J. P.; Jacobsen, K. W. Bayesian Error Estimation in Density-Functional theory. *Phys. Rev. Lett.* **2005**, *95*, 1–4.

(6) Abild-Pedersen, F.; Greeley, J.; Studt, F.; Rossmeisl, J.; Munter, T.; Moses, P. G.; Skulason, E.; Bligaard, T.; Nørskov, J. K. Scaling properties of adsorption energies for hydrogen-containing molecules on transition-metal surfaces. *Phys. Rev. Lett.* **2007**, *99*, 016105.

(7) Viswanathan, V.; Hansen, H.; Rossmeisl, J.; Nørskov, J. K. Universality in Oxygen Reduction Electrocatalysis on Metal Surfaces. *ACS Catal.* **2012**, *2*, 1654–1660.

(8) Bligaard, T.; Nørskov, J. K.; Dahl, S.; Matthiesen, J.; Christensen, C.; Sehested, J. The Brønsted–Evans–Polanyi relation and the volcano curve in heterogeneous catalysis. *J. Catal.* **2004**, *224*, 206–217.

(9) Tripković, V.; Skúlason, E.; Siahrostami, S.; Nørskov, J. K.; Rossmeisl, J. The oxygen reduction reaction mechanism on Pt(111) from density functional theory calculations. *Electrochim. Acta* **2010**, *55*, 7975–7981.